

DISCOVERING MASS CLUMPS IN DISTANT GALAXIES WITH LENSING: THE CASE OF B1422+231

CHARLES R. KEETON¹

Astronomy and Astrophysics Department, University of Chicago
5640 S. Ellis Ave., Chicago, IL 60637
ckeeton@oddjob.uchicago.edu

Submitted to *ApJL*, 30 Nov 2001

ABSTRACT

Substructure in distant gravitational lens galaxies can be detected because it alters the brightnesses and shapes of the lensed images. The optical and radio flux ratios in the four-image lens B1422+231 imply that there is a $\sim 10^4\text{--}10^7 h^{-1} M_\odot$ mass clump in the lens galaxy in front of image A; this is the first constraint on the mass of a particular clump lying in a distant galaxy and detected by its mass. The data also indicate that a small clump, perhaps a star, is passing in front of image B and making the optical flux ratios variable. Both of these hypotheses can be tested with new observations. B1422+231 demonstrates how data at different wavelengths can be used in individual lenses to probe individual mass clumps in distant galaxies.

1. INTRODUCTION

In hierarchical models of structure formation, the amount of substructure in dark matter halos provides an important test of the nature of the dark matter. For cold dark matter (CDM), mass clumps can survive the merger process and halos are predicted to be lumpy (Klypin et al. 1999; Moore et al. 1999); while for alternate types of dark matter (e.g., warm or self-interacting), mass clumps are disrupted during mergers and halos are predicted to be much more smooth (Spergel & Steinhardt 2000; Colin, Avila-Reese & Valenzuela 2000; Bode, Ostriker & Turok 2001). In the Local Group, the number of dwarf galaxy satellites is much smaller than the number of subhalos predicted by CDM, which has been interpreted as a potentially profound problem with CDM (Klypin et al. 1999; Moore et al. 1999). This conclusion is not unambiguous, however. Astrophysical processes such as photoionization can quench star formation in small halos (Bullock, Kravtsov & Weinberg 2000), so the number of detectable satellite galaxies may under-represent the amount of substructure in galaxy halos.

Gravitational lensing offers a better test for substructure because it is directly sensitive to mass. The image brightnesses in strongly lensed systems are very sensitive to small-scale structure in the lens galaxy. Any mass clump, such as a globular cluster, gas cloud, or satellite galaxy, can alter the brightness of an image by an arbitrary amount (relative to a lens where the mass is smoothly distributed; Mao & Schneider 1998; Metcalf & Madau 2001; Chiba 2001; Dalal & Kochanek 2001). Even a clump as small as a star can perturb the images of small sources ($\lesssim 0.1$ pc; e.g., Chang & Refsdal 1979); in this case, the star's orbital motion can also induce variability in the image brightness with a time scale of order months (e.g., Irwin et al. 1989). I use the term “sub-lensing” for the generic phenomenon of strongly lensed images being perturbed by substructure in the lens galaxy, and reserve the term “microlensing” for events in which the time variability is detectable.

The four-image lens B1422+231 is an example of a system where sub-lensing appears to be important. The flux ratios between the images depend on both wavelength and time in a way that is inconsistent with smooth lens models (Keeton, Kochanek & Seljak 1997; Mao & Schneider 1998; Metcalf & Zhao 2001; also see §2). I propose that the wavelength and time dependence imply two distinct sub-lensing events occurring in this system: a relatively massive subhalo in front of image A makes the radio flux ratios differ from the optical flux ratios; and a small object, perhaps a star, passing in front of image B makes the optical flux ratios change with time. The sub-lensing explanation for image A has been considered before (Mao & Schneider 1998; Chiba 2001; Dalal & Kochanek 2001), but only using a statistical treatment to determine whether a plausible collection of mass clumps could explain the radio flux. Here I examine the hypothesis in more detail, using joint fits to the radio and optical data to obtain evidence for, and constraints on, particular objects acting as the perturbers. Section 2 reviews the data for B1422+231 from the literature, Section 3 discusses modeling methods, Section 4 presents results from the models, and Section 5 offers conclusions.

2. DATA

B1422+231 consists of a radio-loud quasar at redshift $z_s = 3.62$ that is lensed into four images by an elliptical galaxies at redshift $z_l = 0.34$ (Patnaik et al. 1992). The lens galaxies lies in a poor group of galaxies that contributes an important tidal shear to the lensing potential (Hogg & Blandford 1994; Kundić et al. 1997). The shapes and polarizations of the images inferred from VLBA observations are fully consistent with lensing (Patnaik et al. 1999). For the lensed images, high-precision astrometry from the VLBA maps yields relative positions with error ellipses roughly 0.2 mas by 0.04 mas (Patnaik et al. 1999). HST imaging yields the relative position of the lens galaxy with an uncertainty of 4 mas (Falco et al., in prep.).

Photometry of the four images has been obtained numerous times at several radio frequencies and in various

¹ Hubble Fellow

optical and near-IR passbands. The most useful data are flux ratios between the images, which are shown in Fig. 1. Flux ratios are independent of the intrinsic flux and variability of the source,² so they should be independent of both time and wavelength in simple lens models (see Schneider, Ehlers & Falco 1992). Contrary to expectations, there is a significant difference between A/C(radio) and A/C(optical) that persists over time. The radio flux ratio has long presented problems for lens models (e.g., Keeton et al. 1997); rather than being a failure of imagination among modelers, the problem is generic to smooth lens models (Mao & Schneider 1998). The flux ratios A/C(optical), A/C(radio), and B/C(radio) are all consistent (at better than 95% confidence) with being constant over at least a 6-year baseline,³ while B/C(optical) appears to have declined in recent years. The data therefore reveal two puzzles in B1422+231. First, why is the A/C flux ratio different at radio and optical wavelengths? Second, why is the B/C flux ratio constant at radio wavelengths and variable at optical wavelengths? I propose that both puzzles can be solved by invoking small-scale structure in the lens galaxy, as explained in §4.

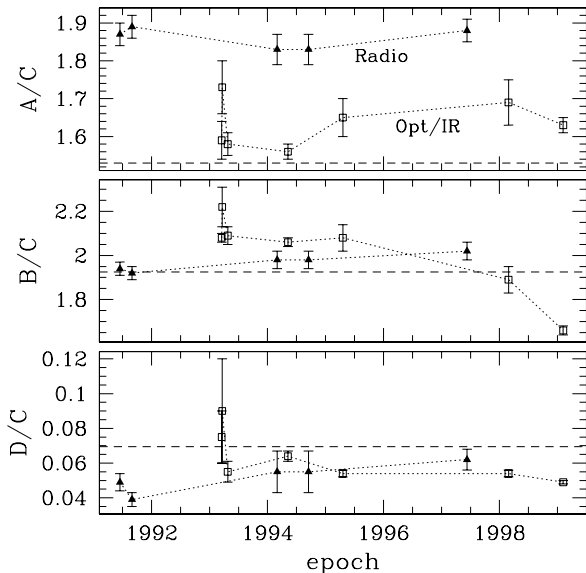


FIG. 1.— Flux ratios for B1422+231 as a function of time. The dashed lines indicate the flux ratios predicted by the macromodel for the lens (see §3). The optical/near-IR data come from Remy et al. (1993), Hammer et al. (1995), Yee & Bechtold (1996), Impey et al. (1996), and Falco et al. (in prep.). The radio data come from Patnaik et al. (1992, 1999) and Patnaik & Narasimha (2001). Differential extinction has little effect on the flux ratios (Falco et al. 1999).

3. MODELING TECHNIQUES

The lensing analysis begins with a smooth lens model, or macromodel, fit to the global properties of the lens. I use a fiducial model consisting of a singular isothermal ellipsoid for the lens galaxy and an external shear to represent the tidal perturbation from the group around the lens galaxy. The model is constrained using the position data only (be-

cause the fluxes are the subject of the sub-lensing analysis). The model gives a very good fit; the image positions are fit arbitrarily well, and the galaxy position is offset by $(\Delta\alpha, \Delta\delta) = (-3.4, -5.2)$ mas giving a total $\chi^2 = 2.4$ for two degrees of freedom. The best-fit lens galaxy has an ellipticity $e = 0.31 \pm 0.02$ at position angle $\theta_e = -56^\circ 1 \pm 0^\circ 2$, with an external shear $\gamma_{\text{ext}} = 0.164 \pm 0.005$ at position angle $\theta_{\gamma, \text{ext}} = -52^\circ 60 \pm 0^\circ 03$. (All uncertainties are at 95% confidence.) Even though the model was not constrained by the image flux ratios, it agrees well with the B/C and D/C flux ratios and slightly underpredicts the A/C optical flux ratio (see Fig. 1). Table 1 gives the convergence κ , the shear amplitude γ and direction θ_γ , and the magnification μ predicted by the macromodel at each image. Other macromodels can be found that predict different values for the convergence and shear at each image. Changes to the macromodel would therefore modify the detailed quantitative results from the sub-lensing analysis — but would not change the main conclusion that sub-lensing is at work in B1422+231.

In a sub-lensing analysis a mass clump is added to the macromodel near one of the images, and the new lens equation is solved to find the properties of the perturbed image. (Clumps lying far from the image can be considered to be part of the macromodel and need not be treated explicitly; see Metcalf & Madau 2001.) The new model is evaluated with a χ^2 statistic defined from the flux ratio data in Fig. 1. I consider two types of mass clumps: a point mass representing highly concentrated clumps, such as individual stars or globular clusters; and a singular isothermal sphere (SIS) representing more extended clumps, such as dwarf galaxy satellites. Other clump models are possible, but these two are sufficient for demonstrating that sub-lensing can explain the puzzles in B1422+231, and for illustrating how the results depend on the clump model.

I assume that the radio and optical emission sources are coincident but have different sizes. Combining the VLBA image shapes (Patnaik et al. 1999) with the macromodel suggests that the radio source is roughly circular with a FWHM of ~ 0.4 mas. The continuum optical emission region in quasars is thought to be $\sim 10^{15}$ cm in size (e.g., Rees 1984; Wyithe et al. 2000), corresponding to $\lesssim 10^{-4}$ mas for the source in B1422+231.

TABLE 1. MACROMODEL RESULTS

Image	κ	γ	θ_γ ($^\circ$)	μ
A	0.384	0.476	-29.0	6.57
B	0.471	0.634	-49.5	-8.26
C	0.364	0.414	-83.1	4.29
D	1.863	2.025	-55.1	-0.30

Note — The angles θ_γ are quoted as position angles measured East of North.

² Provided that the time scale for intrinsic variability is long compared with the time delay between the images, which is true for B1422+231 (e.g., Patnaik & Narasimha 2001).

³ Patnaik & Narasimha (2001) claim to see systematic variations in the 15 GHz radio fluxes during March–September 1994, but the putative variations are smaller than the errorbars.

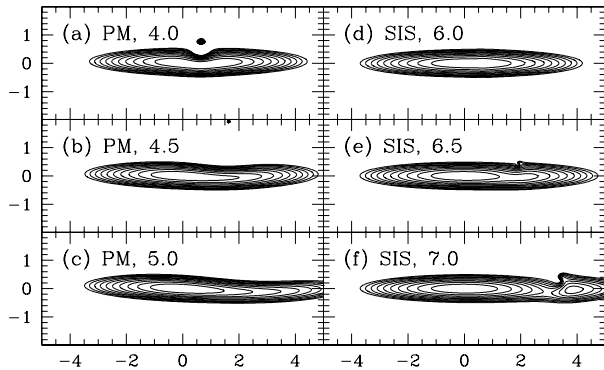


FIG. 2.— Maps of the radio images predicted by various sub-lensing models for image A, assuming infinite resolution. Results are shown for models with a point mass clump (left) and an SIS clump (right); each panel gives the clump mass as $\log M$ (in $h^{-1} M_{\odot}$). The axes are labeled in mas, and the contours are spaced by 0.2 dex.

4. SUB-LENSING RESULTS

4.1. Image A

In the sub-lensing picture for image A, a relatively large mass clump perturbs the radio flux but not the optical flux. Two conditions are required for the picture to work. First, the clump must be massive enough to have an Einstein radius comparable in size to the radio source. Second, the clump must be located at a position where it can affect the radio image but not the optical image — which is possible because the radio image (size $\sim 2.1 \times 0.4$ mas; Patnaik et al. 1999) is so much larger than the optical image (size $\lesssim 10^{-4}$ mas).

Small clumps cannot produce strong enough perturbations to explain the difference between the radio and optical flux ratios, so fits to the data yield lower limits on the clump mass. For fiducial point mass and SIS clumps, the mass limits are (at 95% confidence)

$$M > \begin{cases} 0.9 \times 10^4 (R_{src}/0.4 \text{ mas})^2 h^{-1} M_{\odot} & \text{PM} \\ 1.0 \times 10^6 (R_{src}/0.4 \text{ mas})^{3/2} h^{-1} M_{\odot} & \text{SIS} \end{cases} \quad (1)$$

In this mass range, the time scale for variability due to motion of the clump is several hundred years or longer. The mass limits depend on the clump model because, for a given clump mass, highly concentrated point mass clumps produce larger changes in the lensing potential than more extended SIS clumps. Above these lower limits, the flux data leave a degeneracy between the mass and position of the clump. A more massive clump produces a stronger perturbation, but it can still explain the fluxes if it is moved to a lower surface brightness region of the radio image (keeping the total radio flux fixed).

The mass degeneracy can be broken by adding information about the shape of the radio image. Fig. 2 shows that the image shape depends on the clump mass; more massive clumps produce more substantial distortions. Existing 1 mas resolution VLBA maps do not show visible distortions of the type seen in Figures 2c or 2f (Patnaik et al. 1999), so they imply that the clump mass is not high,

$$M \lesssim \begin{cases} 10^5 (R_{src}/0.4 \text{ mas})^2 h^{-1} M_{\odot} & \text{PM} \\ 10^7 (R_{src}/0.4 \text{ mas})^{3/2} h^{-1} M_{\odot} & \text{SIS} \end{cases} \quad (2)$$

Higher resolution maps will do one of two things. If they do not reveal any shape distortions in image A, they will

disprove the sub-lensing hypothesis as an explanation for the anomalous radio flux ratio in B1422+231. However, if they do show distortions in image A that are not seen in the other images, they will prove the existence of a clump in front of image A. They will permit more sophisticated models to use the image shape to determine the position and mass of the clump. Moreover, because the image shape depends on the nature of the clump (e.g., point mass or SIS; see Fig. 2), it will allow models to determine the mass distribution within the clump. This is an important general result: flux data alone produce mass constraints that depend on the type of clump assumed; but image shapes provide enough additional constraints to determine clump properties like size and density (see Metcalf & Madau 2001 for more discussion).

4.2. Image B

For image B, sub-lensing must produce a variable optical flux ratio without significantly affecting the radio flux ratio. The lack of change in the radio data now gives an upper limit on the clump mass. The optical variability suggests that this may be an example of stellar microlensing — the clump(s) may simply be one or more stars in the lens galaxy. I restrict attention to models where a single clump is responsible for the variability, motivated by two reasons. First, the main goal is to determine whether sub-lensing can explain image B, and it makes sense to start with the simplest possible model to see whether it is sufficient. Second, the image lies far from the center of the lens galaxy where the optical depth for microlensing is small, which is equivalent to saying that sub-lensing is likely to involve a single star.

Fig. 3 shows the χ^2 versus the clump mass for models optimized over the position and velocity of the clump. The data can be fit by a single point mass with any mass $M \lesssim 200 h^{-1} M_{\odot}$. (With a reasonable optical source size of 10^{-4} mas [see §3], finite source size effects do not preclude point mass clumps down to at least $0.1 h^{-1} M_{\odot}$.) Thus, the current data are consistent with microlensing by a single star with a reasonable mass. The data can also be fit by an SIS clump with $100 \lesssim M \lesssim 4000 h^{-1} M_{\odot}$, although in this mass regime the SIS model may be physically implausible.

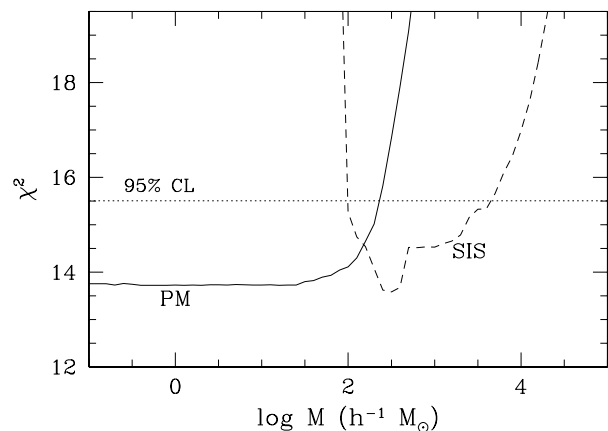


FIG. 3.— The χ^2 versus clump mass for sub-lensing models of image B. The models are optimized over the position and velocity of the clump, so there are 8 degrees of freedom. Results are shown for point mass (PM) and SIS clump models. The dotted line shows the 95% confidence limit.

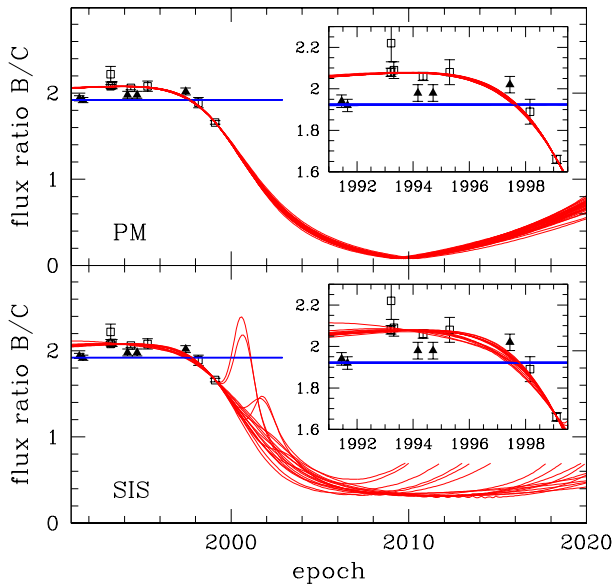


FIG. 4.— The B/C flux ratio as a function of time. The points show the data, while the curves show predictions from all of the models in Fig. 3 that fit the data at better than 95% confidence. The triangles and horizontal lines denote the radio flux ratio, while the squares and curves denote the optical flux ratio. The main panels show an extended time period, while the insets highlight the period spanned by the data.

Fig. 4 shows the B/C flux ratio as a function of time for all of the models that fit the data at better than 95% confidence. Some SIS sub-lensing models predict that image B experienced a caustic-crossing event in the year 2000 or 2001. More robustly, all models predict that the optical flux ratio will continue to decline for several more years, and will soon reach a point where image B is fainter than both images A and C. The fact that sub-lensing *de-amplifies* optical image B is important, and is due to the fact that B is a parity-reversed image. Further monitoring of the B/C optical flux ratio will be very important to test the sub-lensing hypothesis for image B. Measurements several times a year for several years should reveal continued variability, providing improved data and allowing new models to determine whether the variability requires one or many stars. Polarimetric and/or spectral monitoring of the images could even provide constraints on the relative

sizes of the continuum emission and the absorption regions in the source (e.g., Belle & Lewis 2000).

5. CONCLUSIONS

Substructure in the lens galaxy offers the first successful explanation of the wavelength and time dependence in the flux ratios of the lens B1422+231. The difference between the optical and radio flux ratios of images A and C implies a mass clump in front of image A. A highly concentrated clump must have a mass of $\sim 10^4\text{--}10^5 h^{-1} M_\odot$, while a more extended clump must have a mass of $\sim 10^6\text{--}10^7 h^{-1} M_\odot$. This is the first evidence for a particular object of mass $\sim 10^4\text{--}10^7 h^{-1} M_\odot$ lying in a distant galaxy and detected by its mass. Sub-mas resolution radio maps should either confirm the clump and strongly constrain its mass, position, size, and density — or else rule out the clump hypothesis altogether.

The time dependence in the optical flux ratio of images B and C implies that a small mass clump is passing in front of image B; the object could be a normal star, or an extended object of mass $\sim 10^3 h^{-1} M_\odot$. Models with a single clump predict that the B/C optical flux ratio will continue to decline for several more years, so photometric monitoring will test the sub-lensing hypothesis and reveal whether the variability is due to one star or many.

This analysis of B1422+231 complements the recent statistical analyses of lensing and substructure by Dalal & Kochanek (2001) and Chiba (2001). The statistical approach uses flux ratios for an ensemble of lenses to place limits on the statistical properties of subhalo populations, showing that they are consistent with CDM and inconsistent with known satellite populations. By contrast, B1422+231 demonstrates that analysis of more detailed data in individual lenses, including photometry at multiple wavelengths and epochs and high-resolution maps of radio images, can constrain individual mass clumps in distant galaxies.

Support for this work was provided by NASA through Hubble Fellowship grant HST-HF-01141.01-A from the Space Telescope Science Institute, which is operated by the Association of Universities for Research in Astronomy, Inc., under NASA contract NAS5-26555.

REFERENCES

- Belle, K. E., & Lewis, G. F. 2000, *PASP*, 112, 320
 Bode, P., Ostriker, J. P., & Turok, N. 2001, *ApJ*, 556, 93
 Bullock, J. S., Kravtsov, A. V., & Weinberg, D. H. 2000, *ApJ*, 539, 517
 Chang, K., & Refsdal, S. 1979, *Nature*, 282, 561
 Chiba, M. 2001, preprint astro-ph/0109499
 Colin, P., Avila-Reese, V., & Valenzuela, O. 2000, *ApJ*, 542, 622
 Dalal, N., & Kochanek, C. S. 2001, preprint astro-ph/0111456
 Falco, E. E., Impey, C. D., Kochanek, C. S., Lehár, J., McLeod, B. A., Rix, H.-W., Keeton, C. R., Muñoz, J. A., & Peng, C. Y. 1999, *ApJ*, 523, 617
 Hammer, F., Rigaut, F., Angonin-Willaime, M.-C., & Vandersriest, C. 1995, *A&A*, 298, 737
 Hogg, D. W., & Blandford, R. D. 1994, *MNRAS*, 268, 889
 Impey, C. D., Foltz, C. B., Petry, C. E., Browne, I. W. A., & Patnaik, A. R. 1996, *ApJ*, 462, L53
 Irwin, M. J., Webster, R. L., Hewett, P. C., Corrigan, R. T., & Jedrzejewski, R. I. 1989, *AJ*, 98, 1989
 Keeton, C. R., Kochanek, C. S., & Seljak, U. 1997, *ApJ*, 482, 604
 Klypin, A., Kravtsov, A. V., Valenzuela, O., & Prada, F. 1999, *ApJ*, 522, 82
 Kundić, T., Hogg, D. W., Blandford, R. D., Cohen, J. G., Lubin, L. M., & Larkin, J. E. 1997, *AJ*, 114, 2276
 Mao, S., & Schneider, P. 1998, *MNRAS*, 295, 587
 Metcalf, R. B., & Madau, P. 2001, preprint astro-ph/0108224
 Metcalf, R. B., & Zhao, H. 2001, preprint astro-ph/0111427
 Moore, B., Ghigna, S., Governato, F., Lake, G., Quinn, T., Stadel, J., & Tozzi, P. 1999, *ApJ*, 524, L19
 Patnaik, A. R., Browne, I. W. A., Walsh, D., Chaffee, F. H., & Foltz, C. B. 1992, *MNRAS*, 259, 1P
 Patnaik, A. R., Kembell, A. J., Porcas, R. W., & Garrett, M. A. 1999, *MNRAS*, 307, L1
 Patnaik, A. R., & Narasimha, D. 2001, preprint astro-ph/0106104
 Rees, M. J. 1984, *ARA&A*, 22, 471
 Remy, M., Surdej, J., Smette, A., & Claeskens, J.-F. 1993, *A&A*, 278, L19
 Schneider, P., Ehlers, J., & Falco, E. E. 1992, *Gravitational Lenses* (New York: Springer)
 Spergel, D. N., & Steinhardt, P. J. 2000, *Phys Rev Lett*, 84, 3760
 Wytthe, J. S. B., Webster, R. L., Turner, E. L., & Mortlock, D. J. 2000, *MNRAS*, 315, 62
 Yee, H. K. C., & Bechtold, J. 1996, *AJ*, 111, 1007